2017

OES Task 10 WEC Modelling Verification and Validation

Wendt, F

International Energy Agency Ocean Energy Systems Task 10 Wave Energy Converter Modeling Verification and Validation

Fabian Wendt*, Yi-Hsiang Yu*, Kim Nielsen†, Kelley Ruehl‡, Tim Bunnik§, Imanol Touzon¶, Bo Woo Nam‖, Jeong Seok Kim‖, Kyong-Hwan Kim‖, Carl Erik Janson**, Ken-Robert Jakobsen††, Sarah Crowley‡‡, Luis Vega[x], Krishnakumar Rajagopalan[x], Thomas Mathai[xi], Deborah Greaves[xii], Edward Ransley[xii], Paul Lamont-Kane[xiii], Wanan Sheng[xiv], Ronan Costello[xv], Ben Kennedy[xv], Sarah Thomas[xvi], Pilar Heras[xvi], Harry Bingham[xvii], Adi Kurniawan[xviii], Morten Mejlhede Kramer[xviii], David Ogden[xix], Samuel Girardin[xix], Aurélien Babarit[xx], Pierre-Yves Wuillaume[xx], Dean Steinke[xxi], André Roy[xxi], Scott Beatty[xxii], Paul Schofield[xxiii], Johan Jansson[xxiv, xxv], and Johan Hoffman[xxiv]

*National Renewable Energy Laboratory
Golden, Colorado 80401, USA
E-mail: fabian.wendt@nrel.gov, yi-hsiang.yu@nrel.gov
†Ramboll
Copenhagen DK-2300, Denmark
E-mail: kin@ramboll.com
‡Sandia National Laboratories
Albuquerque, New Mexico 87123, USA
E-mail: kelley.ruehl@sandia.gov
§MARIN, Netherlands ¶ Tecnalia, Spain ‖KRISO, South Korea **Chalmers University, Sweden ††EDRMedeso, Norway
‡‡WavEC, Portugal [x]Hawaii Natural Energy Institute, USA [xi]Glosten, USA [xii]Plymouth University, UK
[xiii]Queen's University Belfast, UK [xiv]University College Cork, Ireland [xv]Wave Venture, UK [xvi]Floating Power Plant, Denmark
[xvii]Technical University of Denmark [xviii]Aalborg University, Denmark [xix]INNOSEA, France
[xx]EC Nantes, France [xxi]Dynamic Systems Analysis, Canada
[xxii]Cascadia Coast Research, Canada [xxiii]ANSYS, USA [xxiv]KTH, Sweden [xxv]BCAM, Spain

***Abstract*—This is the first joint reference paper for the Ocean Energy Systems (OES) Task 10 Wave Energy Converter modeling verification and validation group. The group is established under the OES Energy Technology Network program under the International Energy Agency. OES was founded in 2001 and Task 10 was proposed by Bob Thresher (National Renewable Energy Laboratory) in 2015 and approved by the OES Executive Committee EXCO in 2016. The kickoff workshop took place in September 2016, wherein the initial baseline task was defined. Experience from similar offshore wind validation/verification projects (OC3-OC5 conducted within the International Energy Agency Wind Task 30) [1], [2] showed that a simple test case would help the initial cooperation to present results in a comparable way. A heaving sphere was chosen as the first test case. The team of project participants simulated different numerical experiments, such as heave decay tests and regular and irregular wave cases. The simulation results are presented and discussed in this paper.**

***Index Terms*—Wave power, numerical model, verification, validation, code comparison, international cooperation, IEA, OES, Task 10, BEM, CFD, heaving sphere, wave energy**

I. Introduction

Numerical modeling is an important aspect of the design of a wave energy converter (WEC). Designers use different simulation software packages (codes) that predict the response and loads of a WEC during operation and extreme events. These codes are based on different assumptions and numerical modeling approaches. The goal of the International Energy Agency (IEA) Offshore Energy Systems (OES) Task 10 is to gain confidence in using numerical models and assessing the accuracy of these codes. This project will eventually help to improve confidence levels in numerical predictions of power production and load estimates, which are important quantities for the development of reliable and cost-efficient WECs.

A total of 25 different organizations from 11 countries participated in the first phase of this project. The participants include universities, research laboratories, commercial software developers, and WEC developers.

The first phase focused on the relatively simple problem of a heaving, spherical body. The motivation behind the selection of this simplistic modeling problem was mitigating potential

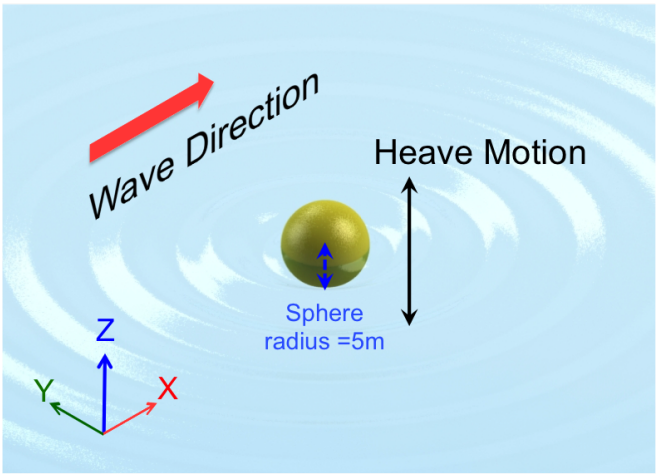

Fig. 1. Illustration of the heaving sphere used in the first phase of the project

issues related to communication, data exchange protocols, and uncertainties in the model definition. Future phases of IEA OES Task 10 will move towards more realistic WEC systems with increased complexity, once the differences and similarities observed for the relatively simple, initial model are sufficiently described and understood.

After presenting the analyzed model and a brief overview of the different participant codes, the authors will discuss the differences observed among the submitted simulation results.

II. Description of Model and Test Cases

A description of the analyzed spherical body and the load cases considered within this project is given below.

A. Model Description

The floating sphere investigated within this project is restrained to heave motion only (Fig. 1). It has a radius of 5.0 m and its origin is located on the mean water surface, at the center of the spherical body. The center of gravity is located 2.0 m below the mean water surface. A summary of the most important model parameters is given in Table I. The hydrodynamic coefficients used in codes that rely on the Cummins equation [3] to predict the motion of the sphere were computed via Nemoh [4] and WAMIT [5] by the National Renewable Energy Laboratory (NREL). MARIN computed their own hydrodynamic coefficients via DIFFRAC [6]. These hydrodynamic coefficients include the diffraction and linear Froude-Krylov forces, as well as information on the frequency-dependent added mass and radiation damping of the body. Based on the analytic solution, the resonance period of the sphere is computed as

$$T_0 = \frac{2\pi}{1.025}\sqrt{\frac{a}{g}}. \tag{1}$$

with g being 9.81 m/s^2 and a being the sphere radius (5.0 m), which yields a resonant period of 4.4 s.

TABLE I
General Properties of the Heaving Sphere

Parameters	Assigned Values
Radius of Sphere	5 m
Initial Sphere Location	$0.0, 0.0, 0.0$ m
Center of Gravity	$0.0, 0.0, -2.0$ m
Mass of Sphere	261.8×10^3 kg
Water Depth	Infinite
Water Density	1000 kg/m^3

B. Description of Analyzed Load Cases

The team simulated three sets of load cases: free-decay tests and regular and irregular wave conditions.

1) Free-Decay Tests: Three free-decay scenarios with different initial displacements (1.0 m, 3.0 m, 5.0 m) were analyzed in this project. No additional power take-off (PTO) damping was considered during the free-decay tests. Project participants were asked to submit 40 s of free-decay time-series data.

2) Regular Wave Conditions: With the goal of analyzing the spherical body during wave excitation for a broad range of wave periods, the team simulated the response of the heaving body for 10 different wave periods. Three different levels of wave steepness and three different model configurations (free, optimum PTO damping, and fixed) were considered for each wave period, yielding a total of 90 regular wave simulations. The wave period and wave height combinations used within this project are summarized in Table II. The wave steepness S (as indicated in Table II) has been computed for deep-water conditions as

$$S = \frac{H}{gT^2} \tag{2}$$

with H being the wave height and T being the wave period. The nonlinearity inherent to the three different wave steepness levels considered within this project is illustrated in Fig. 2. For more nonlinear wave conditions, we expected to see larger differences between simple, linear codes and more complex codes that consider nonlinearities like the instantaneous body position in the wave field, or wave kinematics above the mean sea level.

The optimum PTO damping coefficient (B_{opt}) has been calculated based on linear theory [7]

$$B_{opt} = \lambda\sqrt{1 + \left(\frac{C - \omega^2(m+\mu)}{\omega\lambda}\right)^2} \tag{3}$$

with λ being the radiation damping in heave, C the hydrostatic restoring stiffness, ω the wave frequency in rad/s, m the mass of the sphere, and μ the added mass. The corresponding optimum damping coefficients are summarized in Table III. Project participants were asked to submit 150 s of steady-state simulation data.

TABLE II
SUMMARY OF REGULAR WAVE CONDITIONS

T [s]	f [Hz]	λ [m]	H1 [m] S=0.0005	H2 [m] S=0.002	H3 [m] S=0.01
3.0	0.333	14.04	0.044	0.177	0.883
4.0	0.250	24.96	0.078	0.314	1.570
4.4	0.227	30.20	0.095	0.380	1.899
5.0	0.200	39.00	0.123	0.491	2.453
6.0	0.167	56.16	0.177	0.706	3.532
7.0	0.143	76.44	0.240	0.961	4.807
8.0	0.125	99.84	0.314	1.256	6.278
9.0	0.111	126.36	0.397	1.589	7.946
10.0	0.100	156.00	0.491	1.962	9.810
11.0	0.091	188.76	0.594	2.374	11.870

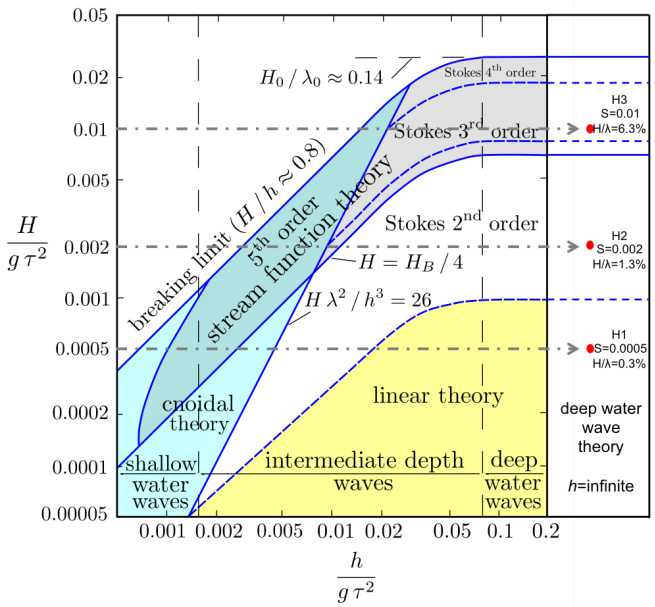

Fig. 2. Analyzed steepnesses and wave theory validity limits, adopted from [8], [9].

TABLE III
OPTIMUM PTO DAMPING FOR REGULAR WAVE CONDITIONS

T [s]	Optimum Damping [Ns/m]	T [s]	Optimum Damping [Ns/m]
3.0	398736.034	7.0	479668.979
4.0	118149.758	8.0	633979.761
4.4	90080.857	9.0	784083.286
5.0	161048.558	10.0	932117.647
6.0	322292.419	11.0	1077123.445

3) Irregular Wave Conditions: In addition to the regular wave conditions, three irregular wave conditions were analyzed in this project. The investigated irregular wave conditions are summarized in Table IV. The first sea state uses a peak spectral period (T_p) that is longer than the resonance period of the sphere. The significant wave height (H_s) of 1 m was selected to achieve a wave steepness ($S = 0.0026$) that is similar to the medium steepness case that was analyzed for the regular wave conditions (S=0.002). For the second irregular wave case, the spectral peak period was set right at the resonance period of the heaving sphere, whereas the significant wave height was chosen to achieve the same wave steepness as the previous irregular wave case. The third irregular wave case represents survival conditions with larger waves and increased steepness; the wave height was limited to avoid the occurrence of breaking waves. For each irregular wave condition, project participants were asked to submit 800 s of simulation data (can include initial transients) with three different model configurations: free floating, prescribed PTO damping, and fixed sphere. For the frequency-domain-based postprocessing of the simulations data, the first 200 s of the simulation were disregarded to minimize the influence of effects related to the model initialization. The prescribed PTO damping values were computed via Equation (3). The authors are aware that these damping values are not optimum in terms of power production for the selected irregular wave conditions; however, they should provide realistic, close-to-optimum damping of the sphere. The selected damping values for the irregular wave conditions are also summarized in Table IV.

TABLE IV
SUMMARY OF IRREGULAR WAVE CONDITIONS AND SELECTED PTO DAMPING COEFFICIENTS

T_p [m]	H_s [s]	γ [-]	S [-]	PTO Damping [Ns/m]
6.2	1.0	1.0	0.0026	398736.034
4.4	0.5	1.0	0.0026	118149.758
15.4	11.0	1.0	0.0047	90080.857

III. DESCRIPTION OF PARTICIPANT CODES

The project participants used a variety of different codes to simulate the response of the heaving sphere. A short summary of each participant and the corresponding code is given below. Each code is labeled with: *<Organization Name>, <Code Name>, <Name tag used for plotting>*.

A. Linear Codes

Linear codes are based on linear wave theory and consider only first-order wave excitation and radiation loads. These tools are widely used in many marine engineering applications to explore large design spaces, because they are computationally inexpensive and numerically robust, and include:

- *NREL-SNL, WEC-SIM, NREL SNL LIN*
- *Dynamic Systems Analysis, ProteusDS, DSA LIN*
- *EC Nantes, Ad-hoc MATLAB code, ECN LIN*
- *Wave Venture, Wave Venture TE, WV LIN*
- *MARIN, aNySIM, MARIN LINS*
- *Tecnalia, MATLAB code, Tecnalia RI*
- *DTU, DTUMotionSimulator, DTU LIN*

- *WavEC, WavEC2Wire, WavEC*
- *Navatek, Aegir, Navatek LINFK*
- *EDRMedeso, ANSYS Aqwa, EDRMedeso LINS*
- *Aalborg University, MATLAB Code, AAU LINS*
- *HNEI, WEC-SIM, HNEI_LIN*
- *KRISO, KIMAPS, KRISO*
- *Innosea, InWave, INNOSEA*
- *Queen's University, MATLAB code, QUB_LIN*.

B. Codes with Weak Nonlinearities

In addition to considering first-order wave-excitation and radiation forces, codes with weak nonlinearities are augmented to consider additional nonlinear effects. Examples for these nonlinearities are the consideration of the instantaneous body position in the wave field, extrapolation of wave kinematics above the mean sea level, and the consideration of quadratic transfer functions for second-order wave-excitation forces. The computational time requirements for these codes are usually higher than for the purely linear codes, but they are often less expensive than codes that are able to capture strong nonlinearities. For each code listed below, the weak nonlinearities that were considered are briefly summarized:

- *NREL, WEC-SIM, NREL SNL NLIN*:
  Nonlinear hydrostatic restoring stiffness and Froude-Krylov forces based on instantaneous body position and wave elevation.
- *Dynamic Systems Analysis, ProteusDS, DSA NLIN*:
  Nonlinear hydrostatic and Froude-Krylov loading computed. Hydrostatic and dynamic fluid pressure is numerically integrated over the wetted surface of the sphere at every time step.
- *EC Nantes, WS_ECN, ECN NLIN*:
  Weak-scatterer method: nonlinear hydrostatic and Froude-Krylov forces and hydrodynamic forces (diffraction and radiation) on exact wetted surface at every time step.
- *Wave Venture, Wave Venture TE, WV NLIN*:
  Modified Cummins equation with nonlinear hydrostatic and Froude-Krylov forces and integrated multibody and mooring analysis.
- *MARIN, aNySIM, MARIN NLINS*:
  Nonlinear hydrostatic and Froude-Krylov forces. Hydrostatic and incident wave pressure is numerically integrated over the wetted surface of the sphere at every time step.
- *DTU, DTUMotionSimulator, DTU NLIN*:
  Exact Froude-Krylov and hydrostatic forcing.
- *Navatek, Aegir, Navatek NLINFK*:
  Nonlinear hydrostatics and Froude-Krylov forces.
- *EDRMedeso, ANSYS Aqwa, EDRMedeso NLINS*:
  Nonlinear hydrostatic and Froude-Krylov loading computed. Hydrostatic and dynamic fluid pressure is numerically integrated over the wetted surface of the sphere at every time step.
- *Glosten, Python Code, glosten*:
  Nonlinear hydrostatics for the free-decay test, purely linear modeling approach for wave cases.
- *University College Cork, UCC_TD, UCC*:
  Nonlinear force is added for the restoring force, because of the different horizontal sectional areas.
- *HNEI, WEC-SIM, HNEI_NLIN*:
  Nonlinear Froude-Krylov and restoring forces calculated from wave elevation and instantaneous position of body
- *WavEC, WavEC2Wire, WavEC NLINS*:
  Nonlinear hydrostatic and Froude-Krylov forces calculated from the instantaneous body position and wave elevation.

C. Codes with Strong Nonlinearities

Codes that consider strong nonlinearities include both computational fluid dynamics (CFD) and fully nonlinear time-domain boundary element models, which are able to capture the shape of very steep and highly nonlinear waves. The CFD models can also capture wave impact and breaking effects. These codes are computationally expensive to run and are often used to analyze specific extreme events.

- *Chalmers University, SHIPFLOW-MOTIONS, Chalmers*:
  Fully nonlinear potential flow boundary element method solved in the time domain.
- *NREL-SNL, StarCCM+, NREL_SNL_CFD*:
  Time-step size $dt = 0.01 - 0.015$ s, URANS with k-ω SST turbulent model using an overset mesh.
- *EDRMedeso, ANSYS Fluent, EDRMedeso_CFD*:
  Explicit volume of fluid method with dynamic mesh approach, adjustable time step, no turbulence model.
- *Plymouth University, Open Foam, PU*:
  RANS with no turbulence model, an irregular, deforming mesh, and an adjustable time step based on a maximum Courant number of 0.5.
- *KTH-BCAM, Unicorn/FEniCS-HPC, KTH*:
  Variable-density Direct FEM with no turbulence model, fixed mesh, dt = 0.000725.

IV. Discussion of Simulation Results

A discussion of the simulation results is given here. The identification of systematic differences in the simulation results and their connection to differences in modeling approaches are the main focus of the data analysis. Some of the participant results presented in the following section diverge significantly from the other participants. Commenting on individual outliers is beyond the scope of this paper and requires detailed knowledge of the utilized code and modeling approach. The authors recommend further follow-on analysis conducted by the respective participants to investigate potential differences in numerical predictions observed within this project.

A. Free-Decay Tests

The three free-decay tests (initial heave displacements: 1.0 m, 3.0 m, and 5.0 m) were simulated only for 40 s, which allowed a large variety of codes (including high-fidelity tools

with extensive computational costs) to participate in the code-to-code comparison.

The time series for the 1.0-m and 5.0-m case are shown in Figures 3–4. For the case with the 1.0-m initial displacement, all codes agree well and no significant differences in the predicted heave response can be observed.

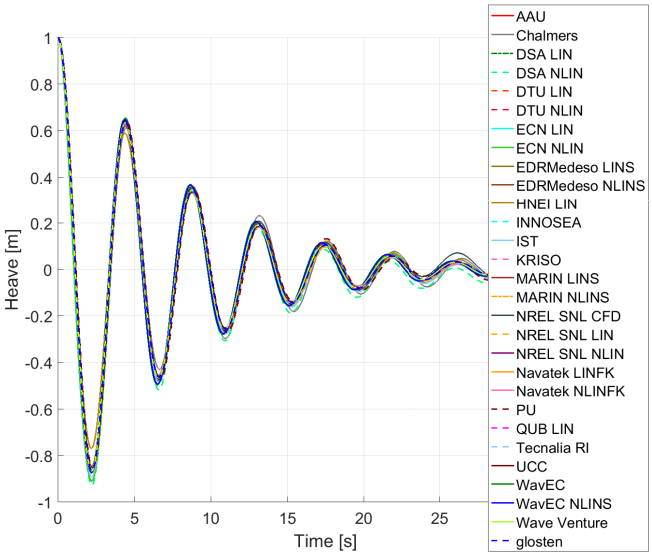

Fig. 3. Free-decay response in heave for the 1.0-m initial displacement.

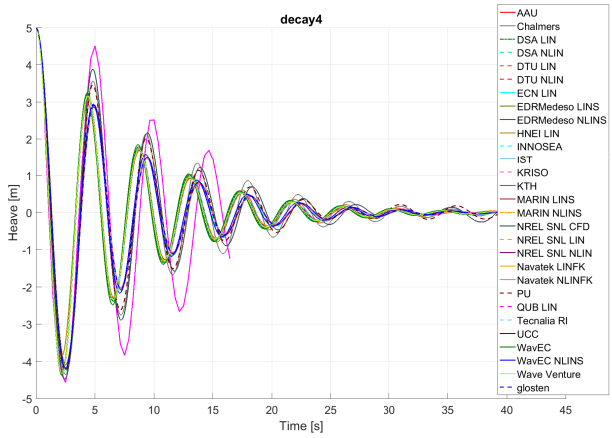

Fig. 4. Free-decay response in heave for the 5.0-m initial displacement.

For the case with 5.0-m initial displacement, there is a clear separation between linear codes and codes with weak nonlinearities (Figure 4). The group that is leading in phase consists of *DSA NLIN, DTU NLIN, EDRMedeso NLINS, IST, MARIN NLINS, NREL SNL NLIN, Navatek NLINFK, WavEC NLINS*, and *glosten*. All these weakly nonlinear codes consider the instantaneous body position for calculating the hydrostatic restoring force. The influence of this effect is most prominent for large amplitude motions. Because the water plane area of the sphere will change with its position relative to the mean sea level, this geometric nonlinearity will have the largest

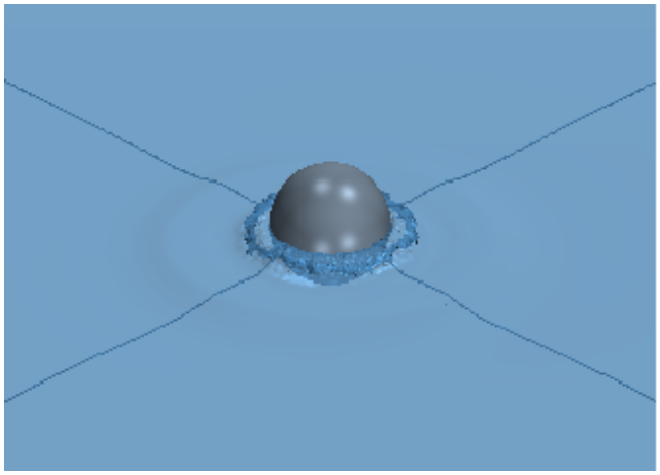

Fig. 5. Breaking radiated waves during large amplitude heave motion (from *the NREL SNL CFD* solution).

influence during the first, large oscillations of the sphere. From 0 s to about 20 s, differences in motion amplitude can be observed between purely linear codes and the codes with weak nonlinearities.

The third group that is evident in the heave response for the relatively large initial displacement of 5.0 m are the codes with strong nonlinearities: *NREL SNL CFD*, *PU*, *KTH*, and *Chalmers*. The phase of the solution from these three models is close to the phase of the codes with weak nonlinearities. However, these three codes predict a larger motion amplitude than the rest of the group. In the three codes with strong nonlinearities, instead of using a linear radiation assumption like the weakly nonlinear codes, they are able to capture higher-order wave radiation effects, which are largely influenced by the instantaneous sphere cross section area at the water surface, particularly at the first oscillation of the free-decay case with the 5.0-m initial displacement. In addition, during the first oscillation, the *NREL SNL CFD* solution predicts breaking of the radiated wave around the sphere (Figure 5), an effect that can only be captured by CFD models. It is also worth mentioning that the relatively good agreement between the time-domain potential flow code from *Chalmers* and the CFD solutions (*NREL SNL CFD* and *PU*) suggests that the effect of fluid viscosity and wave breaking on the body response plays a relatively small role in the analyzed scenario.The KTH-BCAM results are not mesh-converged, but there is an evident trend towards increased decay with finer discretization, consistent with the difference in results to the other CFD groups.

The computational resources utilized for the free decay simulations with 5.0 m initial displacement are summarized in Table V. The comparison of computational resources was not conducted in a controlled environment, meaning each participant used their own computer system. The computational time obviously depends on the hardware specifics of each system, which is why the presented numbers on simulation time should be interpreted with caution.

TABLE V
UTILIZED COMPUTATIONAL RESOURCES FOR FREE DECAY SIMULATION.

Participant	**Number of CPU Cores [-]**	**Simulation Time [s]**
NREL	1	6.0
NREL NLIN	1	20.0
NREL CFD	160	2.63E5
DSA LIN	1	66.0
DSA NLIN	1	493.0
AAU	1	0.3
KRISO	1	5.0
HNEI LIN	1	120.0
ECN LIN	1	1.2
DTU LIN	1	10.8
DTU NLIN	1	11.1
WAVEC	4	5.0
PU	9	5.6E5
Tecnalia RI	4	8.0
QU	4	1.0
UCC	1	18.24
INNOSEA	1	4.3
WAVE VENTURE	1	0.1

B. Regular Wave Conditions

The group simulated 30 different regular sea states (as summarized in Table II), and three different model configurations (free, optimum PTO damping, and fixed). This yields a total of 90 simulations for each participant.

To achieve a reasonable frequency resolution for further frequency-domain-based postprocessing, the participants were asked to submit 150 s of steady-state data. Because of the large number of simulations and relatively long simulation time, no significant simulation data for codes with strong nonlinearities were submitted.

For the first two levels of steepness ($S = 0.0005$ and $S = 0.002$), no major differences were observed among the different codes. The heave-motion response amplitude operator (RAO) plot for $S = 0.002$ is shown in Figure 6. The RAO for each regular wave condition is computed as

$$RAO = \sqrt{m_{peak}/\zeta_{peak}} \tag{4}$$

with m_{peak} being the first-order peak of the heave-motion power spectral density (PSD) and ζ_{peak} being the first-order peak of the wave elevation PSD.

Figures 7–8 illustrate the heave RAO for the large steepness regular wave cases ($S = 0.01$), with and without PTO damping, respectively. Starting from a wave period of around 6 s, codes with nonlinear hydrostatics and nonlinear-Froude-Krylov forcing predict a reduced heave response for the case with optimum PTO damping. This reduction is caused by geometric nonlinearities that come into effect when increasing ratios of wave height over sphere diameter.

Such a difference in heave response is not observed for the case without PTO damping (free-floating sphere), as seen in Figure 8. This outcome is likely because in long waves the free-floating sphere behaves more as a wave follower, which mitigates nonlinearities induced by changes in relative position between the instantaneous free-water surface and the heaving sphere.

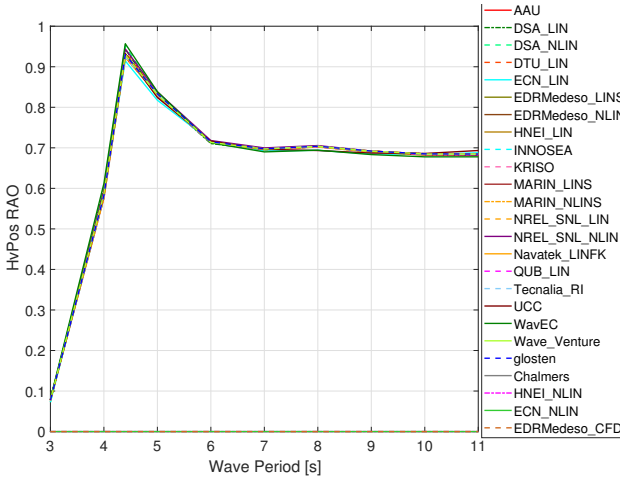

Fig. 6. Heave RAO, optimum PTO damping, S=0.002.

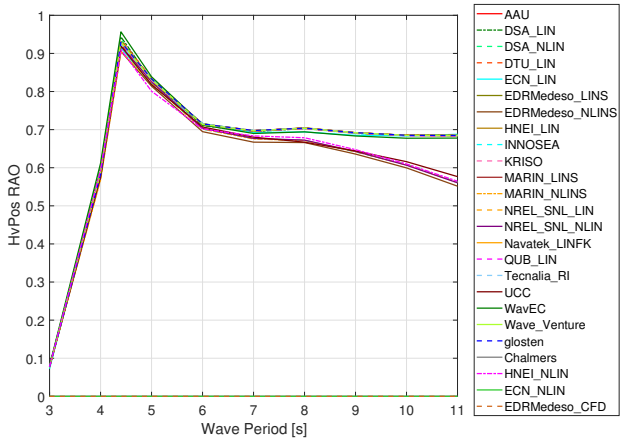

Fig. 7. Heave RAO, optimum PTO damping, S=0.01.

As shown in Equation (4), the RAO value only contains information about the first-order response of a system. To investigate potential higher-order system responses, an analysis of the PSD over a broader frequency range is necessary. Figure 9 shows the heave-motion PSD for a wave period of 4.4 s, with a wave height of 0.095 m. This case has a relatively low-wave steepness of $S = 0.0005$ and is within the linear wave condition. Besides the first-order peak at 0.2267 Hz, no significant higher-order peaks are present. Purely linear codes and codes with weak nonlinearities show good agreement.

Increasing the wave height from 0.095 m to 1.899 m for the same wave period of 4.4 s yields a steepness of $S = 0.01$. Because of the increased wave height and steepness, nonlinear effects become more important. As shown in Figure 10, in addition to the first-order peak at 0.2267 Hz, the codes with

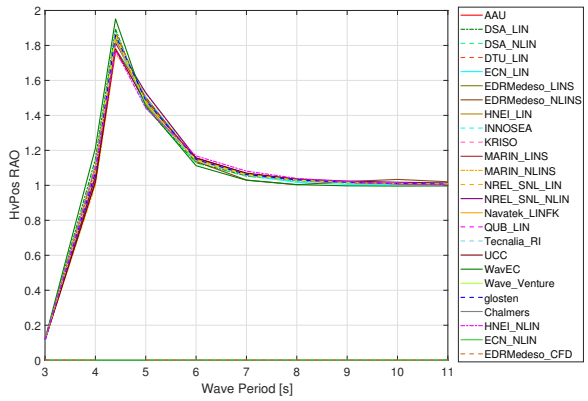

Fig. 8. Heave RAO, no PTO damping, S=0.01.

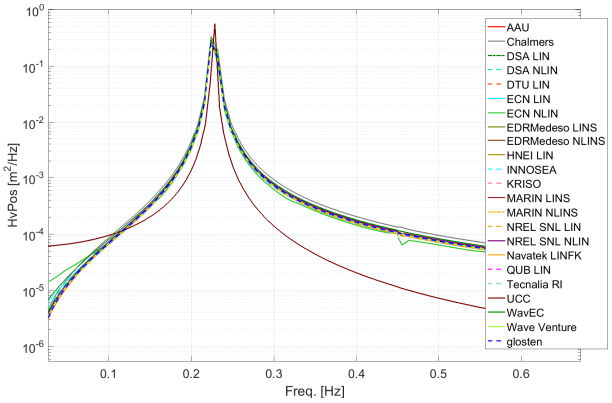

Fig. 9. Heave PSD, T=4.4 s, H=0.095 m, no PTO, $S = 0.0005$.

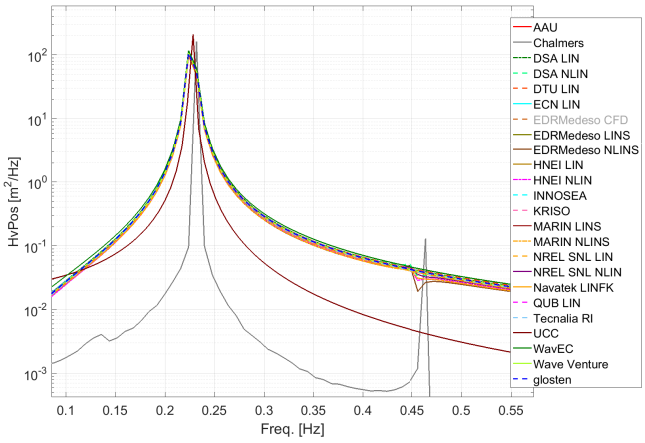

Fig. 10. Heave PSD, T=4.4 s, H=1.899 m, no PTO, $S = 0.01$.

weak or strong nonlinearities—*EDRMedeso NLINS, HNEI NLIN, MARIN NLINS, NREL SNL NLIN*, and *Chalmers*—show a noticeable second-order peak at about 0.45 Hz.

On the other hand, keeping the steepness at $S = 0.01$, but moving towards larger waves and therefore larger ratios of wave height over sphere diameter adds extra higher-order peaks to the PSD of the heave motion (Figure 11). Codes with weak nonlinearities that predict these higher-order peaks are *HNEI NLIN, MARIN NLIN, DSA NLIN*, and *NREL SNL NLIN*.

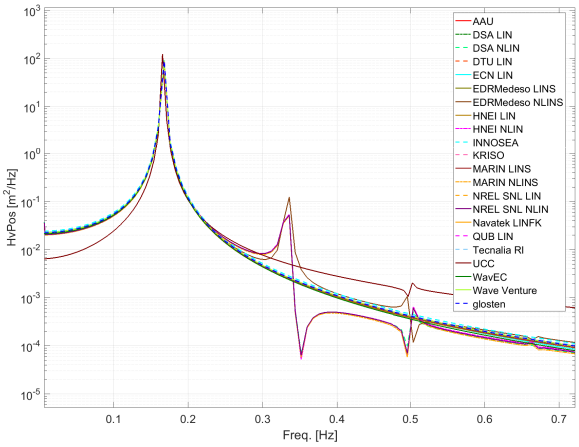

Fig. 11. Heave PSD, T=6.0 s, H=3.532 m, optimum PTO damping, $S = 0.01$.

Comparing the mean power normalized by the wave height squared for optimum PTO damping yields good agreement between the linear codes and the codes with weak nonlinearities for a wave steepness of $S = 0.0005$, as shown in Figure 12. For a steepness of $S = 0.01$, the codes with weak nonlinearities predict a lower mean power value for wave periods above 7 s (Figure 13). This prediction is consistent with what was observed for the heave RAO for steep waves (Figure 7). Codes with weak nonlinearities that show a reduced mean power for larger waves are *UCC, HNEI NLIN, EDRMedeso NLINs, DSA NLIN, MARIN NLINS, and NREL SNL NLIN*. The mean power output is mainly controlled by the first-order peak, which is smaller for codes with weak nonlinearities during wave conditions that have a relatively large wave-height-to-sphere-diameter ratio.

C. Irregular Wave Conditions

Three different irregular wave scenarios have been investigated, and the given conditions are listed in Table IV. Because of the relatively long simulation time of 800 s, as for the regular wave cases, no simulation data from codes with strong nonlinearities were submitted for analysis. Although the regular wave analysis was based on the comparison of RAOs, the irregular wave analysis is based on the direct comparison of power spectral density (PSD) plots, of the sphere's heave-0motion response.

As for the regular wave results with low wave steepness, no significant differences were observed among the purely linear codes and the codes with weak nonlinearities. For the irregular wave train with increased steepness ($S = 0.0047$, Figure 14), the codes with weak nonlinearities (*NREL SNL NLIN, UCC, DSA NLIN*) predict a larger heave response for frequencies above and below the linear wave-excitation region. However, as for the regular waves, the codes with weak nonlinearities predict a smaller first-order peak for the heave response. A direct comparison of the heave-motion PSD for the linear

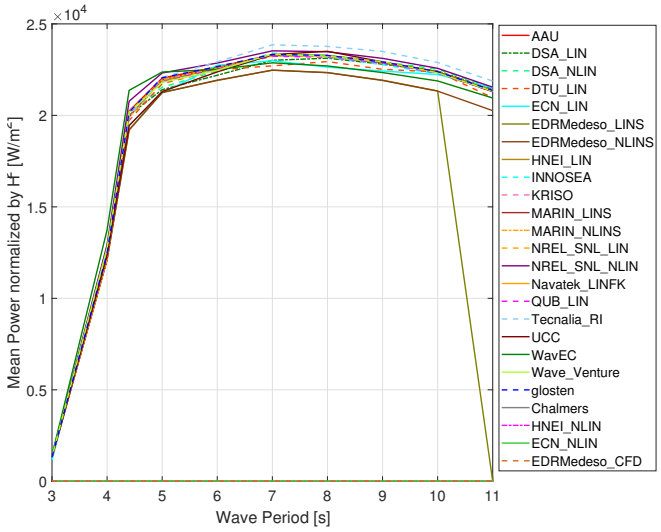

Fig. 12. Mean power normalized by the square of the wave height, $S = 0.0005$, optimum PTO damping.

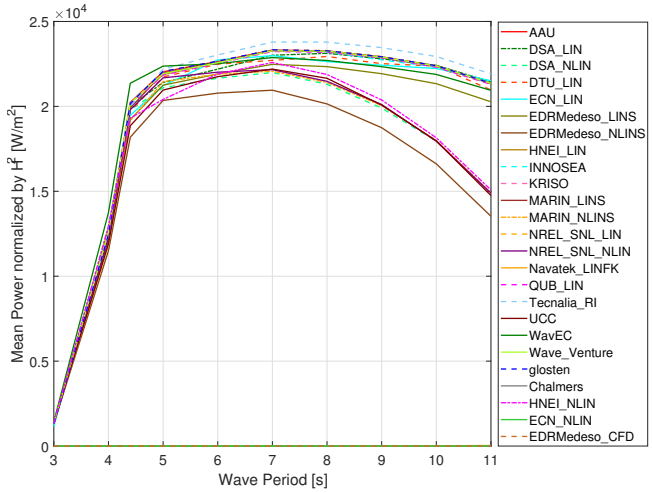

Fig. 13. Mean power normalized by the square of the wave height, $S = 0.01$, optimum PTO damping.

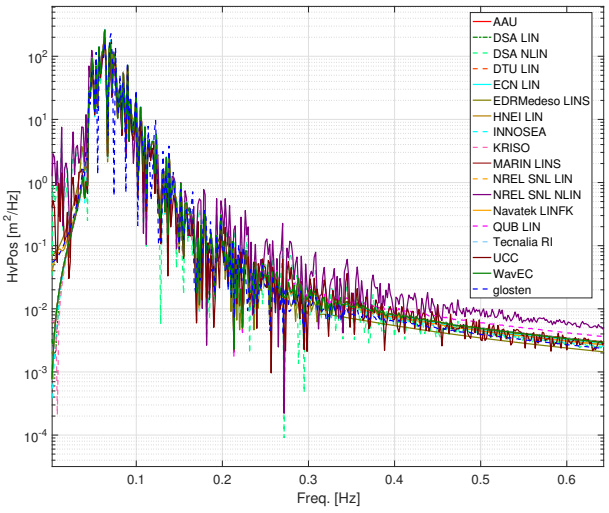

Fig. 14. Heave motion PSD, T_p=15.4 s, H_s=11 m, optimum PTO damping.

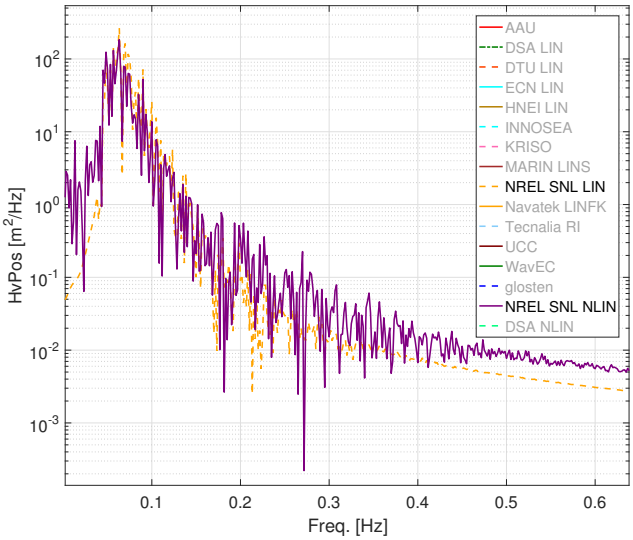

Fig. 15. Heave-motion PSD, T_p=15.4 s, H_s=11 m, optimum PTO damping, NREL SNL solutions only.

solution and the solution with weak nonlinearities for *NREL SNL* is shown in Figure 15.

Regarding the power production, as for the regular waves, the mean power appears to be mainly controlled by the linear wave-excitation region. Figure 16 shows the bar plot of the mean power for the irregular wave case with steep waves ($S = 0.0047$). It reveals that the solutions with weak nonlinearities (*NREL SNL NLIN, UCC, DSA NLIN*) all show a reduced mean power output, compared to the overall average of the linear solutions.

V. Conclusion

During the course of the first phase of IEA OES Task 10, different codes (linear codes and those with weak and strong nonlinearities) were verified based on a direct code-to-code comparison. The group of participants compared the response of a heaving sphere in deep water during free-decay tests and regular and irregular wave tests. For the free-decay analysis, clear differences in amplitude and phasing between the linear codes, codes with strong nonlinearities, and codes with weak nonlinearities were observed for the test case with the largest initial displacement (5.0 m). The other free-decay tests with initial displacements of 1.0 m and 3.0 m showed no significant differences between modeling approaches.

For codes with weak nonlinearities, the nonlinear hydrostatics caused a phase shift in the motion response. Codes with strong nonlinearities that consider higher-order wave-radiation forces also showed increased motion amplitudes, especially during the large initial oscillations of the sphere.

For the regular wave conditions, only simulation data for

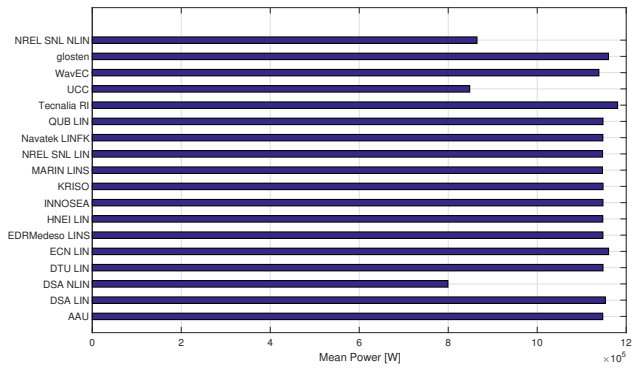

Fig. 16. Mean power for the irregular wave case, with T_p=15.4 s, H_s=11 m, optimum PTO damping.

linear codes and codes with weak nonlinearities were submitted (because of the relatively large number of simulations, the longer simulated time, and the high computational expenses associated with the codes with strong nonlinearities). Between the linear codes and those with weak nonlinearities, differences in system response were observed for the regular wave conditions with high wave steepness ($S = 0.01$). An analysis of the heave PSD for these regular wave cases with steep waves revealed that the codes with weak nonlinearities are able to capture higher-order peaks in the heave PSD because of the consideration of nonlinear hydrostatics and Froude-Krylov forcing, whereas the purely linear codes were only able to capture the first-order peak. For regular wave conditions with large waves, the first-order peak of the heave response for codes with weak nonlinearities fell below what was predicted by the purely linear codes. Consequently, the codes with weak nonlinearities predict a reduced mean power output for regular wave conditions with large, steep waves because of the consideration of nonlinearities in hydrostatics and Froude-Krylov forcing. These effects become more important for large waves as a result of the geometric nonlinearities related to the spherical shape of the simulated body.

Similar observations were made during the analysis of the irregular wave conditions. For conditions with low steepness waves, no significant differences between the linear codes and those with weak nonlinearities were observed. However, for wave conditions with large, steep waves, the codes with weak nonlinearities showed additional excitation below and above the predominant wave-excitation frequencies, but a reduced response at these frequencies. As for the regular wave conditions, this effect translates into a reduced mean power output for the codes with weak nonlinearities, caused by geometrically induced nonlinearities, which are captured through the consideration of nonlinear hydrostatics and Froude-Krylov forcing.

VI. Future Work Within IEA OES Task 10

Moving forward, the IEA OES Task 10 project will focus on a second round of code-to-code comparison with the heaving sphere. Additional model properties will be introduced to move the behavior of the sphere closer to the characteristics of an actual WEC (e.g., motion end stops, nonlinear PTO damping). The introduction of focused wave load cases that enables the analysis of large nonlinear survival wave conditions with a relatively short simulated time is being considered as well. This approach will be especially interesting for codes with strong nonlinearities and high computational expenses. The group will discuss further on the details of these additional model specifications and load cases.

Model validation based on actual wave tank data is currently envisioned for the next phase of the project. The self-reacting point-absorber data set presented in [10] has been identified as a potential candidate for the first validation phase of IEA OES Task 10, because of its simplicity and thorough documentation.

Acknowledgments

IEA OES Task 10 is initiated under the technology collaboration program for Ocean Energy Systems (OES) under the framework established by the International Energy Agency in Paris. The support from OES to host the workshops and initiate the work is acknowledged. In-kind contribution and support offered by the participating institutions are acknowledged and the significant work done by NREL in compiling and analyzing the results is acknowledged and only possible via the support by the U.S. Department of Energy under Contract No. DE-AC36-08GO28308 with the National Renewable Energy Laboratory. Funding for the work was provided by the DOE Office of Energy Efficiency and Renewable Energy, Water Power Technologies Office.

References

[1] J. M. Jonkman, A. Robertson, W. Popko, and *et al.* , "Offshore code comparison collaboration continuation (OC4), phase I: Results of coupled simulations of an offshore wind turbine with jacket support structure," in *Proc. of the 22nd International Offshore and Polar Engineering Conference*, Rhodes, Greece, 2012.

[2] A. N. Robertson, F. Wendt, J. Jonkman, and *et al.* , "OC5 project phase I: Validation of hydrodynamic loading on a fixed cylinder," in *Proc. of the 25th International Offshore and Polar Engineering Conference*, Kona, Hawaii, 2015.

[3] W. Cummins, "The impulse response function and ship motions," *Schiffstechnik*, vol. 9, pp. 101–9, 1962.

[4] A. Babarit and G. Delhommeau, "Theoretical and numerical aspects of the open source BEM solver NEMOH," in *Proc. of the 11th European Wave and Tidal Energy Conference*, Nantes, France, 2015.

[5] WAMIT, "WAMIT, the state of the art in wave interaction analysis," http://www.wamit.com/, 2016.

[6] T. Bunnik, W. Pauw, and A. Voogt, "Hydrodynamic analysis for side-by-side offloading," in *Proc. of the 19th International Offshore and Polar Engineering Conference*, Osaka, Japan, 2009.

[7] N. M. Tom, M. J. Lawson, Y. H. Yu, and A. D. Wright, "Development of a nearshore oscillating surge wave energy converter with variable geometry," *Renewable Energy*, vol. 96, no. A, pp. 410–424, 2016.

[8] B. Le Mehaute, *An introduction to hydrodynamics and water waves*. New York: Springer-Verlag, 1976.

[9] Wikipedia, "Stokes wave — Wikipedia, the free encyclopedia," 2017, [Online; accessed 11-April-2017]. [Online]. Available: https://en.wikipedia.org/w/index.php?title=Stokes_wave&oldid=765177969

[10] S. J. Beatty, "Self-reacting point absorber wave energy converters," Ph.D. dissertation, University of Victoria, Victoria, BC, Canada, 2015.